# Adhesion between silica surfaces due to hydrogen bonding

James Bowen,[1*] Hebert L Rossetto,[2] Kevin Kendall[2]

[1] Department of Engineering and Innovation, The Open University, Walton Hall, Milton Keynes, MK7 6AA, UK

[2] School of Chemical Engineering, The University of Birmingham, Edgbaston, Birmingham, B15 2TT, UK

* To whom correspondence should be addressed

Email: james.bowen@open.ac.uk

Telephone: + 44 (0) 1908 655 614

**Abstract**

The adhesion between surfaces can be enhanced significantly by the presence of hydrogen bonding. Confined water at the nanoscale can display behaviour remarkably different to bulk water due to the formation of hydrogen bonds between two surfaces. In this work we investigate the role of confined water on the interaction between hydrophilic surfaces, specifically the effect of organic contaminants in the aqueous phase, by measuring the peak adhesive force and the work of adhesion. Atomic force microscope cantilevers presenting hemispherical silica tips were interacted with planar single crystals of silica in the presence of dimethylformamide, ethanol, and formamide; solution compositions in the range 0-100 mol% water were investigated for each molecule. Each molecule was chosen for its ability to hydrogen bond with water molecules, with increasing concentrations likely to disrupt the structure of surface-bound water layers. With the exception of aqueous solutions containing low concentrations of ethanol, all molecules decreased the ability of confined water to enhance the adhesion between the silica surfaces in excess of the predicted theoretical adhesion due to van der Waals forces. The conclusion was that adhesion depends strongly on the formation of a hydrogen-bonding network within the water layers confined between the silica surfaces.

**Keywords**

Adhesion, atomic force microscopy, dimethylformamide, ethanol, formamide, silica, water

## 1. Introduction

The structure and dynamics of water is a highly studied interdisciplinary research topic, of interest to scientists and engineers from many different disciplines. Water is essential for life on Earth and exhibits unique properties that mediate a wide range of physical, chemical, and biochemical processes [1]. The anomalous and fascinating properties of liquid water [2] arise from the tendency of neighboring molecules to form hydrogen bonds, which when formed serve to decrease the local potential energy and entropy, and impose a structure to the molecule network. The dimensions and double-donor double-acceptor capacity of water molecules gives them a unique flexibility to form a variety of hydrogen bonds. Confinement tends to distort the way water organizes itself, and so do contaminants, which affect the role of confined water.

The structure and properties of water under nanoconfinement has relevance to generating understanding of biological mechanisms, such as biomolecule interactions [3-5] including protein folding [6-7], cell/surface adhesion [8-9], antibody/antigen complexation [10], and biomineralization [11]. There is significant research activity in this field which undertakes simulation work, including molecular dynamics. There is also significant recent work involving infra-red spectroscopy [12] and NMR [13] which studies the role of water on the properties of lysozyme.

This paper investigates the role of confined water on the adhesion of hydrophilic surfaces. Atomic force microscopy (AFM) [14] is used to probe the adhesion of two silica surfaces in the presence of water ($H_2O$) and the organic molecules dimethylformamide (DMF), ethanol (EtOH), and formamide (FA). These molecules, all have the ability to hydrogen bond with $H_2O$ molecules, and each other. The behaviour of these solutions when under nanoconfinement will affect the adhesion between the surfaces. Hence, it is possible to mimic the interactions involved in many of the biologically important processes outlined above, using a measurement technique, AFM, which is increasingly of benefit to researchers worldwide in a variety of fields.

## 2. Methods

### 2.1 Solution preparation

Laboratory grade dimethylformamide (DMF), ethanol (EtOH), and formamide (FA) (Sigma-Aldrich, UK) were mixed with HPLC grade water (Fisher Scientific, UK) to create solutions where the mole fraction of organic varied from 0-100%. The range of solutions created is listed in **Table 1**. The refractive indices and dielectric constants for the solutions were calculated according to the relations proposed by Heller [15] and Raju [16] respectively.

| Solution | Water content (mol%) | Organic content (mol%) | Refractive index, n (-) | Dielectric constant, $\varepsilon$ (-) | Density, $\rho$ (kg/m$^3$) |
|---|---|---|---|---|---|
| $H_2O$ | 100 | 0 | 1.33 | 80.0 | 1,000.0 |
| | | | | | |
| $DMF_1$ | 0.05 | 99.95 | 1.33 | 79.9 | 999.9 |
| $DMF_2$ | 0.2 | 99.8 | 1.33 | 79.6 | 999.5 |
| $DMF_3$ | 2.0 | 98.0 | 1.34 | 75.9 | 995.8 |
| $DMF_4$ | 20.0 | 80.0 | 1.38 | 55.9 | 971.8 |
| $DMF_5$ | 33.3 | 66.7 | 1.40 | 49.4 | 962.5 |
| $DMF_6$ | 50.0 | 50.0 | 1.41 | 44.7 | 955.1 |
| $DMF_7$ | 66.7 | 33.3 | 1.42 | 41.7 | 950.1 |
| $DMF_8$ | 80.0 | 20.0 | 1.42 | 40.1 | 947.2 |
| $DMF_9$ | 0.0 | 100.0 | 1.43 | 38.3 | 944.0 |
| | | | | | |
| $EtOH_1$ | 99.8 | 0.2 | 1.33 | 79.5 | 998.9 |
| $EtOH_2$ | 98.0 | 2.0 | 1.33 | 75.3 | 989.7 |
| $EtOH_3$ | 80.0 | 20.0 | 1.34 | 49.7 | 917.7 |
| $EtOH_4$ | 50.0 | 50.0 | 1.35 | 33.7 | 848.3 |
| $EtOH_5$ | 20.0 | 80.0 | 1.36 | 26.9 | 807.8 |
| $EtOH_6$ | 0.0 | 100.0 | 1.36 | 24.3 | 789.0 |
| | | | | | |
| $FA_1$ | 99.8 | 0.2 | 1.33 | 80.0 | 1,000.7 |
| $FA_2$ | 98.0 | 2.0 | 1.33 | 80.2 | 1,006.3 |
| $FA_3$ | 80.0 | 20.0 | 1.37 | 81.4 | 1,051.2 |
| $FA_4$ | 50.0 | 50.0 | 1.41 | 82.7 | 1,095.0 |
| $FA_5$ | 20.0 | 80.0 | 1.43 | 83.6 | 1,120.9 |
| $FA_6$ | 0.0 | 100.0 | 1.44 | 84.0 | 1,133.0 |

**Table 1.** Composition, refractive index, dielectric constant, and density of the prepared solutions at 18 $^o$C.

### 2.2 Atomic force microscopy adhesion measurements

Atomic force microscopy (AFM) adhesion measurements were performed using a NanoWizard II AFM (JPK Instruments, UK). Measurements were performed at identical fixed end approach and retract velocities of 2.0 µm/s. When retracting the tip from the substrate surface, the tip stays near to the surface until the force stored in the cantilever, due to tensile deflection, overcomes the adhesive tip-sample interaction. Each force measurement represents the mean of 64 points probed across an area of 100 x 100 µm on a single crystal silica substrate (5 x 5 x 0.5 mm, both sides polished to $R_a$ = 0.5 nm, Pi-Kem Ltd, UK). The cantilever was developed by NanoWorld AG (Switzerland) to present a 2.0 µm radius silica hemisphere at its apex. The thickness and spring constants of the cantilevers were obtained according to the method previously described by Bowen *et al*. [17]. The frequency of the first resonant mode of each cantilever was measured,

at 18 °C and 40% relative humidity. Thus, a sphere-on-flat geometry system is employed to investigate the interaction between two silica surfaces. Adhesion measurements were performed in liquid media at 18 °C, with both the substrate and the cantilever fully submerged. The compositions of the liquid media are given in **Table 1**. The Force-Displacement data acquired were analysed in order to provide (i) the peak force, and (ii) the adhesion energy, during the 'tip/surface approach' and 'tip/surface retract' phases of the measurement.

## 2.3 Adhesion

The theoretical work of adhesion, $W_{th}$, for the sphere-on-flat interaction between the AFM cantilever tip and the planar substrate surface was calculated according to **Eq. 1** [18]. This is also termed the 'adhesion energy'.

$$W_{th} = -\frac{AR}{6D} \tag{1}$$

where, $A$ is the Hamaker constant, $R$ is the radius of the AFM cantilever tip, and $D$ is the minimum separation distance between the tip and substrate. The derivation of this equation involves an important simplification, whereby $R \gg D$, which is the case for the experiments presented in this work. For the contact pressures it was possible to generate using these cantilevers, a minimum separation distance of $D = 0.25$ nm was used for calculating the theoretical work of adhesion.

The Hamaker constant, $A$, is calculated according to **Eq. 2**, where $A$ is Boltzmann's constant, $T$ is temperature, $h$ is Planck's constant, $\nu_e$ is the main electronic absorption frequency of the system. $\varepsilon$ and $n$ are respectively the static dielectric constant and the refractive index of two identical phases 1 interacting across a medium 3. The silica surfaces were assumed to have a dielectric constant of 4.4 and a refractive index of 1.54. [19]

$$A = \frac{3}{4}kT\left(\frac{\varepsilon_1-\varepsilon_3}{\varepsilon_1+\varepsilon_3}\right)^2 + \frac{3h\nu_e}{16\sqrt{2}}\frac{(n_1^2-n_3^2)^2}{(n_1^2+n_3^2)^{3/2}} \tag{2}$$

## 3. Results

### 3.1 AFM measurements

Typical data acquired during AFM adhesion measurements is shown in **Fig. 1**. The vertical deflection of the cantilever free end during the tip/surface approach (blue) and tip/surface retract (red) are displayed together, as a function of the cantilever fixed end displacement. **Fig. 1(a)** shows data recorded for the $SiO_2/H_2O/SiO_2$ system, in which an out-of-contact repulsive force is visible on the approach data. This repulsive force appears at a displacement of 150 nm, and continues until the minimum separation between the two $SiO_2$ surfaces is achieved, at a displacement of <20 nm. The repulsion is likely due to overlapping counterion clouds as the two $SiO_2$ surfaces are brought increasingly closer together. Upon retraction, the two $SiO_2$ surfaces are kept in close proximity by adhesive forces, until finally the cantilever free end 'snaps' free, at a displacement of 200 nm; the peak adhesive force is approximately 35 nN.

With reference to the solutions listed in **Table 1**, the data recorded for the $SiO_2/FA_6/SiO_2$ system, i.e. pure FA, is shown in **Fig. 1(b)**. In this data there a smaller out-of-contact repulsive force on the tip/surface approach, which begins at a displacement of 80 nm. Similarly, the adhesive force on retraction is much smaller than for $SiO_2/H_2O/SiO_2$, exhibiting a magnitude of <1 nN. Out-of-contact repulsive forces such as those recorded for $SiO_2/H_2O/SiO_2$ were also recorded for $SiO_2/SiO_2$ adhesion studied under the solutions $DMF_1$ to $DMF_6$, $EtOH_1$ to $EtOH_3$, and $FA_1$ to $FA_3$.
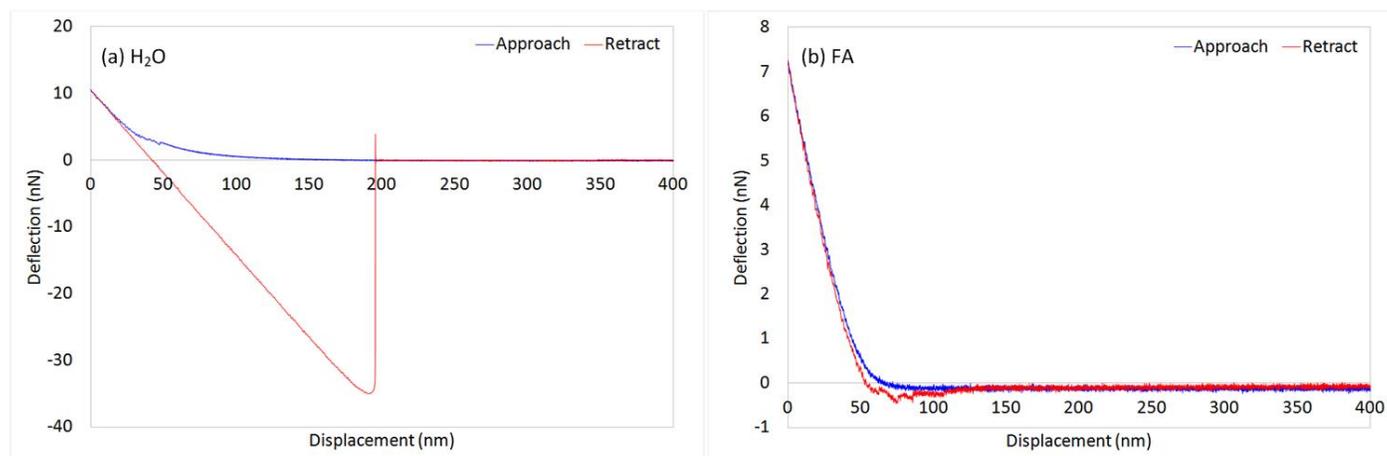


**Figure 1.** Force-displacement plots for (a) $SiO_2/H_2O/SiO_2$ and (b) $SiO_2/FA_6/SiO_2$ interactions measured using AFM.

### 3.2 Effect of dielectric constant

The dielectric constants of the solutions analysed are presented in **Table 1**. The smallest dielectric constant is 24.3 for $EtOH_6$, i.e. pure EtOH, whereas the largest dielectric constant is 84.0 for $FA_6$, i.e. pure FA. This parameter serves as a useful variable to compare the nature of the $SiO_2/SiO_2$ adhesive interaction in the range of solutions tested. **Fig. 2** shows how (a) peak adhesion force, and (b) adhesion energy vary as a function of the solution dielectric constant, for the tip/surface approach. Each peak force in **Fig. 2(a)** is recorded directly from the acquired AFM data, whereas the values of adhesion energy in **Fig. 2(b)** are obtained by integrating the force-displacement data, i.e. the 'area under the curve'.

**Fig. 2(a)** shows that the highest peak forces are recorded for aqueous solutions containing <2.0 mol% EtOH, closely followed by $H_2O$. Solutions with dielectric constants $\varepsilon$ <50 and $\varepsilon$ >80 exhibited the lowest peak forces. **Fig. 2(b)** shows that all adhesion energies during the approach were <1 fJ, with EtOH-containing solutions generally exhibiting the highest values.
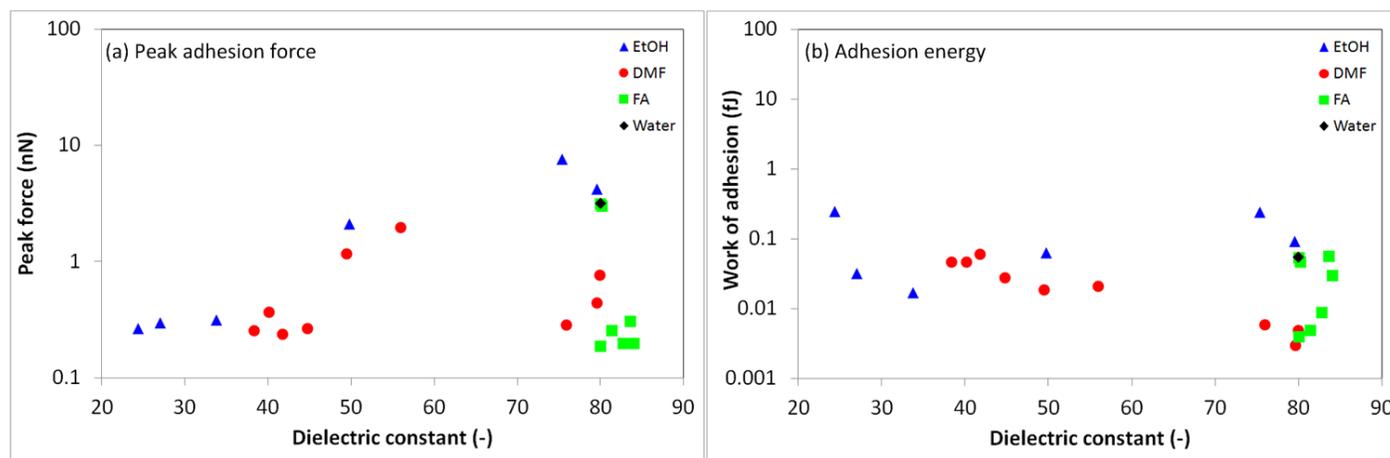


**Figure 2.** $SiO_2/SiO_2$ interaction for tip/surface approach as a function of solution dielectric constant; (a) peak adhesion force, (b) adhesion energy.

**Fig. 3** reveals that the $SiO_2/SiO_2$ adhesive interaction is markedly different for the tip/surface retract when compared to the tip/surface approach. Both the peak force and adhesion energy plots, **Figs. 3(a)** and **3(b)** respectively, show an increase in the magnitude of the adhesive interaction as the dielectric constant increases from $\varepsilon = 50$ to $\varepsilon = 80$. The highest peak forces recorded are on the order 90 nN, and the highest adhesion energies on the order 30 fJ, once again for solutions containing small quantities of EtOH. For $\varepsilon >$ 80 the magnitude of the adhesive interaction decreases rapidly with increasing dielectric constant. **Fig. 3(b)** also shows the theoretical adhesion energy for each $SiO_2$/solution/$SiO_2$ system investigated; these values were calculated using **Eq. 1**. The calculated values do not exceed 20 aJ, and are 1-3 orders of magnitude smaller than the measured values.
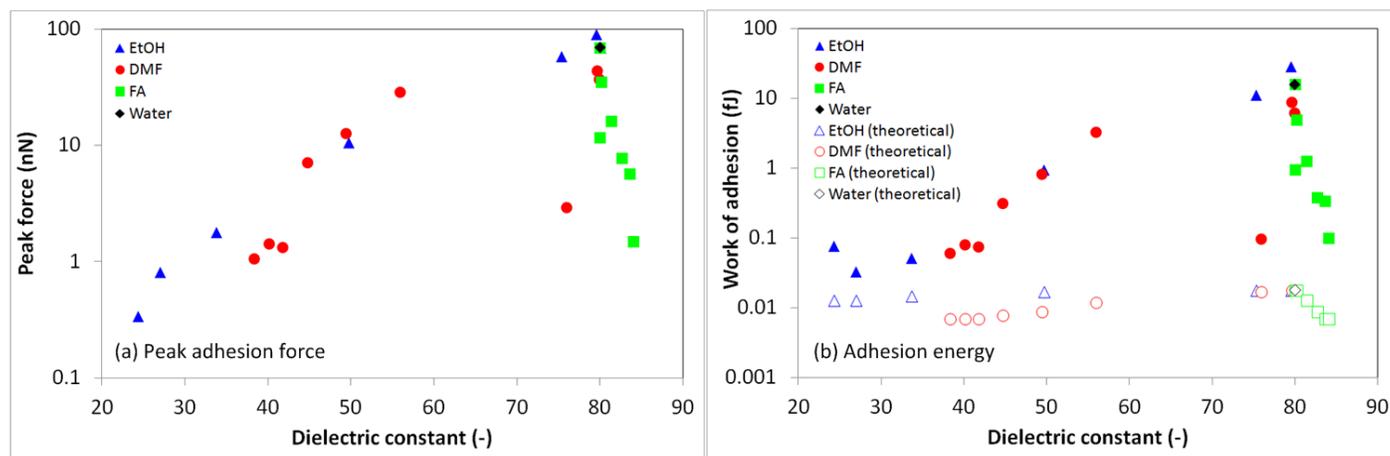


**Figure 3.** $SiO_2/SiO_2$ interaction for tip/surface separation as a function of solution dielectric constant; (a) peak adhesion force, (b) adhesion energy.

## 4. Discussion

The effect of solution dielectric constant on $SiO_2/SiO_2$ adhesion shown in **Fig. 3(b)** is comparable to the effect of solution dielectric constant on $Al_2O_3/Al_2O_3$ adhesion, reported previously [20]. However, in the work presented here it is small amounts of EtOH which enhance the $SiO_2/SiO_2$ adhesive interaction, whereas for $Al_2O_3/Al2O_3$ it was small amounts of DMF which enhanced the adhesion. Both systems show an increase in the magnitude of the adhesive interaction as the dielectric constant increases from $\varepsilon = 50$ to $\varepsilon = 80$, followed by a rapid decrease in the magnitude of the adhesive interaction decreases for $\varepsilon > 80$. Previous measurements performed using $Al_2O_3$ surfaces did not yield out-of-contact repulsive forces for any of the solutions tested. The relatively low viscosities and densities of the solutions investigated, and the low velocity chosen during AFM measurements (2.0 µm/s) mean that the Reynolds number for fluid flow around the hemispherical cantilever tip is very small, and no hydrodynamic or viscous contribution to the adhesion would be expected.

Measured values of adhesion energy were far in excess of the calculated values, which is attributable to the formation of hydrogen bonded networks of $H_2O$ molecules between the surfaces, once they have been brought close together during the tip/surface approach. Hydrogen bonds are directional and strongly attractive, with $H_2O$ molecules exhibiting tetrahedral co-ordination. The ability of DMF, EtOH, and FA to form one or more hydrogen bonds with $H_2O$ molecules is the reason underlying the changes in adhesive behaviour as a function of solution dielectric constant. However, predicting the nature and magnitude of the adhesion for a given solution composition is currently a difficult undertaking. Concentrations of DMF and EtOH in excess of 20 mol% were sufficient to significantly attenuate the adhesion found for the $SiO_2/H_2O/SiO_2$ system. Similarly, FA concentrations of 2.0 mol% and above were sufficient to reduce the adhesion between $SiO_2$ surfaces. It is of great interest that low EtOH concentrations were able to slightly enhance the adhesive interaction.

The peak force and work of adhesion plots in **Figures 2 and 3** display considerable hysteresis between the tip/surface approach and the tip/surface separation, particularly in the dielectric constant range $\varepsilon > 40$. The peak force and work of adhesion are much smaller on the tip/surface approach than on the tip/surface retract. Hence, it is only during the tip/surface retract that there is a resistance to tip/surface separation. This is because a relatively fixed network of hydrogen bonded water molecules has formed between the tip and surface at their closest approach. It then requires significant energy to disrupt this network, thus increasing the entropy of the solution in the tip/sample junction. During the tip/surface approach, the hydrogen bonded network of water molecules has not yet formed, and the tip is simply moving through the unstructured liquid. As the concentration of DMF, EtOH, or FA increases, corresponding to decreased dielectric constant, the hydrogen bonding network is increasingly disrupted. Therefore, the hysteresis between the tip/surface approach and tip/surface retract diminishes because there is less structure to the liquid which undergoes disruption during tip/surface separation.

Elucidating the structure of the hydrogen-bonded $H_2O$ molecule network should be the primary focus of any future work which seeks to investigate the $SiO_2/SiO_2$ or $Al_2O_3/Al_2O_3$ adhesion under aqueous and organic liquid media. The structure of surface-bound solvent molecules co-ordinated at the inorganic surface should

be resolved, as well as the number density of bonds which can be formed per unit area. It should then be possible to construct a theoretical hydrogen bonding network between two surfaces. The energy required to disrupt this network could then be compared to the AFM results presented in this paper. Further, the introduction of contaminant molecules to the network, and their likely influence on the adhesion, could then be studied.

**5. Conclusion**

Confined water at the nanoscale can display behaviour remarkably different to bulk water due to the formation of hydrogen bonds between two surfaces. The adhesion between silica surfaces is enhanced significantly by the presence of hydrogen bonding, with adhesion energies measured using atomic force microscopy several orders of magnitude greater than the theoretical van der Waals adhesion energy. The presence of the organic contaminants dimethylformamide, ethanol, and formamide in the aqueous phase decreased the ability of confined water to enhance the adhesion between the silica surfaces. Aqueous solutions containing low concentrations of ethanol increased the adhesion energy slightly beyond that measured with water, which will be studied in greater detail in future work. The sphere-on-flat methodology presented here provides a valuable tool for studying this phenomenon in greater detail for a wide range of surfaces and solutions. The geometry of the system also assists in the creation of models and simulations, as the hemispherical tip is locally flat at its point of closest approach to the countersurface, with respect to the dimensions of the solvent molecules under investigation.

**Conflict of interest**

The authors declare no competing financial interest.

**Author Contributions**

The manuscript was written through contributions of all authors. All authors have given approval to the final version of the manuscript.

**Funding sources**

**Acknowledgment**

## References

1. Kuwajima, K.; Goto, Y.; Hirata, F.; Kataoka, M.; Terazima, M. (Eds); Water and Biomolecules: Physical Chemistry of Life Phenomena, *Springer-Verlag (Berlin, Germany)*, **2009**.
2. Stanley, H.E.; Kumar, P.; Xu, L.; Yan, Z.; Mazza, M.G.; Buldyrev, S.V.; Chen, S-H.; Mallamace, F.; *Physica A*, **2007**, *386*, 729-743.
3. Kumar, P.; Han, S.; Stanley, H.E.; *J. Phys. Condens. Matter.*, **2009**, *21*, 504108.
4. Stanley, H.E.; Buldyrev, S.V.; Kumar, P.; Mallamace, F.; Mazza, M.G.; Stokely, K.; Xu, L.; Franzese, G.; *J. Non-Cryst. Solids*, **2011**, *357*, 629-640.
5. Mallamace, F.; Corsaro, C.; Mallamace, D.; Stanley, H.E.; Chen, S-H.; *Adv. Chem. Phys.*, **2013**, *152*, 263-308.
6. Mallamace, F.; Corsaro, C.; Mallamace, D.; Baglioni, P.; Stanley, H.E.; Chen, S-H.; *J. Phys. Chem. B*, **2011**, *115*, 14280-14294.
7. Mallamace, F.; Baglioni, P.; Corsaro, C.; Chen, S-H.; Mallamace, D.; Vasi, C.; Stanley, H.E.; *J. Chem. Phys.*, **2014**, *141*, 165104.
8. Curtis, A.S.G.; Forrester, J.V.; McInnes, C.; Lawrie, F.; *J. Cell. Biol.*, **1983**, *97*, 1500-1506.
9. Bella, J.; Humphries, M.J.; *BMC Struct. Biol.*, **2005**, *5*, 4.
10. Yokata, A.; Tsumoto, K.; Shiroishi, M.; Kondo, H.; Kumagai, I.; *J. Biol. Chem.*, **2003**, *278*, 5410-5418.
11. Duer, M.; Veis, A.; *Nature Mater.*, **2013**, *12*, 1081-1082.
12. Mallamace, F.; Corsaro, C.; Mallamace, D.; Vasi, C.; Cicero, N.; Stanley, H.E.; *Front. Phys.*, **2015**, *10*, 106104.
13. Mallamace, F.; Corsaro, C.; Mallamace, D.; Cicero, N.; Vasi, C.; Dugo, G.; Stanley, H.E.; *Front. Phys.*, **2015**, *10*, 108201.
14. Binnig, G.; Quate, C.F.; Gerber, C.; *Phys. Rev. Lett.*, **1986**, *56*, 930-933.
15. Heller, W.; *J. Phys. Chem.*, **1965**, *69*, 1123-1129.
16. Raju, G.R.G.; Conference on Electrical Insulation and Dielectric Phenomena Annual Report, *IEEE (New York, USA)*, **1988**.
17. Bowen, J.; Cheneler, D.; Walliman, D.; Arkless, S.G.; Zhang, Z.; Ward, M.C.L.; Adams, M.J.; *Meas. Sci. Technol.*, **2010**, *21*, 115106.
18. Israelachvili, J.N.; Intermolecular and Surface Forces, 3rd Edition, *Academic Press*, **2011**.
19. Haynes, W.M. (Ed); CRC Handbook of Chemistry and Physics, 92nd Edition, *CRC Press (Boca Raton, USA)*, **2011**.
20. Rossetto, H.L.; Bowen, J.; Kendall, K.; *Langmuir*, **2012**, *28*, 4648-4653.